Phase-Field Modeling of Electromigration-Mediated Morphological Evolution of Voids in Interconnects

by

Sree Shivani Vemulapalli

A Thesis Presented in Partial Fulfillment
of the Requirements for the Degree
Master of Science

Approved April 2020 by the
Graduate Supervisory Committee:

Kumar Ankit, Chair
Nikhilesh Chawla
Arunima Singh

ARIZONA STATE UNIVERSITY

May 2020

ABSTRACT

Miniaturization of microdevices comes at the cost of increased circuit complexity and operating current densities. At high current densities, the resulting electron wind imparts a large momentum to metal ions triggering electromigration which leads to degradation of interconnects and solder, ultimately resulting in circuit failure. Although electromigration-induced defects in electronic materials can manifest in several forms, the formation of voids is a common occurrence. This research aims at understanding the morphological evolution of voids under electromigration by formulating a diffuse interface approach that accounts for anisotropic mobility in the metallic interconnect. Based on an extensive parametric study, this study reports the conditions under which pancaking of voids or the novel void 'swimming' regimes are observed. Finally, inferences are drawn to formulate strategies using which the reliability of interconnects can be improved.

DEDICATION

To my grandfather, Dr. K. N. Rao, who's immense love and support helped me become the person that I am today. From the most insignificant decisions in my life to every life-changing decision, you have stood by my side like a rock and taught me to believe in myself. You have, are, and will always be the most important person in my life.

To my parents, grandmother, and brother without whom I wouldn't have been able to achieve my goals. You helped me sail through my toughest times and made life seem so easy.

ACKNOWLEDGMENTS

I would firstly like to thank my professor, Dr. Kumar Ankit for giving me an opportunity to explore this field of phase-field modeling. Thank you for guiding me throughout this entire journey and believing in me. I am grateful to my committee members at ASU, Dr. Nikhilesh Chawla and Dr. Arunima Singh for agreeing to evaluate my dissertation research. I would like to thank Dr. Alexis Lewis and the National Science Foundation for providing us with the financial support to conduct this research through the award # 1763128.

I would like to thank my colleagues, especially William, for the constant support and help throughout this project. Thank you for being there and motivating me to complete this project. Thank you Rahul for always giving me valuable inputs and offering to help me during my preparation for presentations and meetings. Thank you Ankita and Peichen for all the help and support.

Lastly, I would like to thank my parents, grandparents, and brother for their unconditional love and support. Thank you for inspiring me to become a better person.

TABLE OF CONTENTS

LIST OF TABLES

LIST OF FIGURES

LIST OF FIGURES CONTINUED

Chapter 1

INTRODUCTION

With the current efforts aimed at miniaturizing electronic devices, interconnect reliability has become a major concern. Downscaling of microelectronic devices to the nanometer length scale increases the chances of failure due to a high current density. Certain failure mechanisms that were neglected earlier due to large structural dimensions have become important while designing small-scale electronic devices. Enhancement of atomic migration is one such mechanism which is widely being investigated these days [3, 4, 5].

An enhanced atomic migration refers to a constrained movement of atoms under the influence of an external field. This phenomenon manifests via (i) diffusion down the concentration gradient, (ii) thermal diffusion due to temperature gradient, (iii) atomic migration mediated by mechanical stress, and (iv) electromigration caused due to presence of an electric potential gradient. The research reported in this thesis focuses on electromigration and its effects on interconnect reliability.

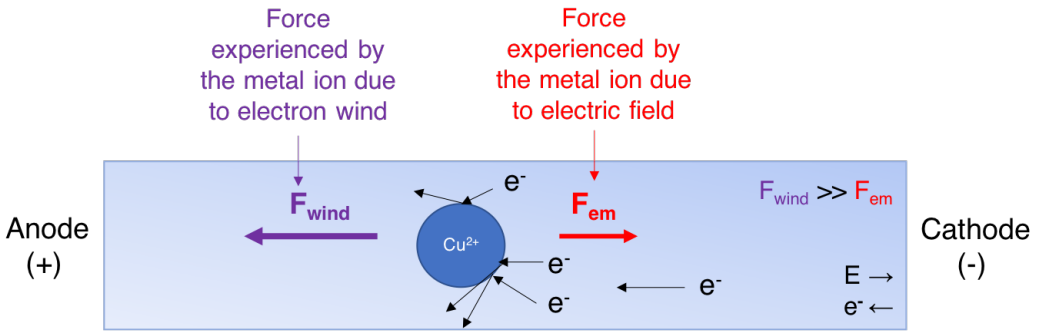

Figure 1.1: Schematic Diagram Showing the Forces Acting on a Metal Ion under the Influence of an Applied Electric Field.

When a large current passes through the interconnect, there are two types of forces acting on the metal ions: an electrostatic force F_{el} due to the strength of the electric field, and a second force F_{wind} caused by the electron wind, as shown in Figure 1.1. The force exerted by a sea of electrons is referred to as electron wind,

F_{wind}. Since the metal ions are shielded by the electrons to an extent, F_{el} is negligible. However, electrons moving across the interconnect tend to collide with metal ions and exchange momentum. When a sufficiently large electric current is passed through an interconnect, the electron wind gains enough momentum to surpass the activation energy of metal ions and knock them out, forcing them to move in the direction of electron wind. This eventually results in the drifting of metal ions from the cathode towards the anode.

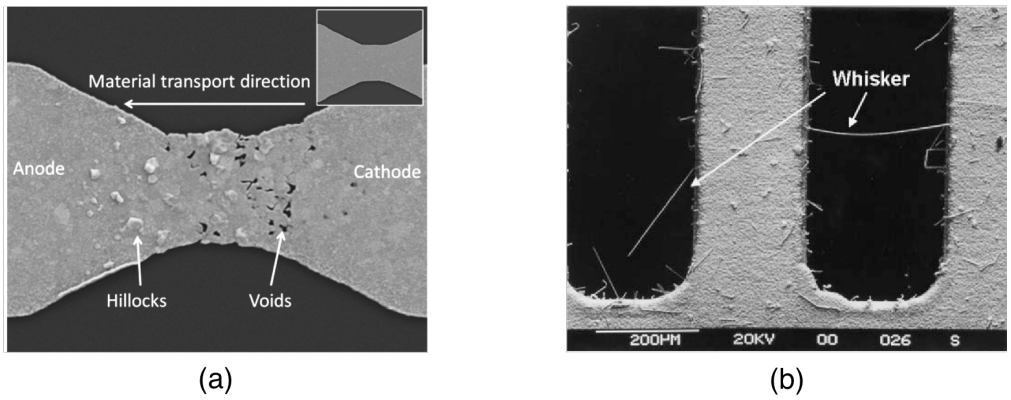

Figure 1.2: Types of Defects Observed in a Metal Interconnect under Electromigration: (a) Voids and Hillocks, and (b) Whiskers [1, 2].

Electromigration results in various types of defects as shown in Figure 1.2. When metal ions start accumulating at one end (say, anode), they pile up on top of each other and form a hill-like structure on the surface, known as a hillock [6, 7, 8]. Hillocks amplify resulting in unwanted electrical connections which ultimately causes a short-circuit.

With the metal ions drifting towards the anode end, tensile stress develops on the cathode end. To relieve the stress, a void is nucleated at this end of the interconnect which continues to grow till the interconnect fails [9]. In case of preexisting voids, the voids diffuse towards the cathode end and accumulate over time, leading to failure of

the interconnect [10, 11, 12].

Another type of defect due to electromigration is the formation of whiskers. This is a metallurgical phenomenon that involves the formation of tiny, thin hair-like structures at the metal surface. Commonly, they lead to arcing and short circuits in the integrated circuits (IC) [13].

In 1966, technological leaders like IBM and Texas Instruments started observing failure in integrated circuits that were manufactured. Although the reason remained unclear for a while, it was eventually found that the failure was caused by electromigration. In the following years, billions of dollars were spent on research aimed at mitigating electromigration in order to increase the reliability of the integrated circuits. One of the key changes that was made in interconnect design was the replacement of aluminum with copper. In the late 1980s, a certain line of desktop drives of Western Digital failed due to electromigration. This caused a huge loss to the company and the engineers had to change their design rules to reduce the impact of electromigration on their devices.

Prior to 1966, aluminum was commonly used as an interconnect material. However, due to its high susceptibility to electromigration, researchers started incorporating small volumes of copper into the interconnects. Although this slowed down the diffusion of metal atoms, it did not solve the problem completely. IBM then proposed a complete switch to copper interconnects and began testing the resistance of new line of copper interconnects to electromigration. Due to its higher conductivity and lower susceptibility to electromigration, copper replaced aluminum as the choice of material for interconnects in electronic devices. Since then, electromigration has gained key importance and researchers continue to study the effects of electromigration on interconnect reliability even today. Although, electromigration in principle can never be completely suppressed, current research focuses on ways to retard the failure rate.

It has previously been reported that electromigration in copper interconnects occurs primarily through the mechanism of void nucleation and growth [14, 15]. According to Gan et al., time-to-failure of copper interconnects mainly depends on void growth time [14]. It is evident that the mitigation of void growth in copper interconnects is critical for enhancing the reliability of ICs. Therefore, the objective of the following research is to gain a fundamental understanding of the morphological evolution of voids in copper interconnects under electromigration.

Past research efforts have focused on experimental characterization of electromigration mediated formation and growth of voids [10, 16, 17], hillocks [18] and whiskers [19]. Mario et al. used SEM to study the impact of preexisting voids in copper interconnects [10] while Jung and Yu studied Kirkendall void growth using backscattered electrons in SEM [20]. Khomich et al. used SEM, Raman spectroscopy and PL to analyze hillocks on homoepitaxial CVD diamond films while Liu et al. used TEM to study the growth of single-crystalline Tin whiskers [18, 19]. However, these tools are quite expensive and it is difficult to observe and record the formation and evolution of voids *in situ*.

With the recent advancements in high-performance computing, simulations techniques have become an effective tool in the study of defects in metal interconnects [20, 21, 22]. There are various types of simulation techniques among which the meshed geometry method is most commonly used. The mesh elements use basic geometries which simplifies the calculations. Such methods can be classified into: finite element method (FEM), finite volume method (FVM), and finite differences method (FDM). Out of these methods, FDM solutions are the most efficient. In the industry, quick simulations are needed, while the simulations may have to be repeated several times in the process of design verification. Therefore, using effort-intensive methods like FEM and FVM is not favored. Hence, FDM is considered to be an effective tool in

the study of defects and interconnect reliability.

By using the finite differences method in a phase-field model, one can visualize and solve free-boundary problems [23, 24, 25]. The boundary conditions applied on domain edges while the evolution equations for the phase-field obtained using variational principles ensure minimization of the total free energy. Phases are designated using a phase-field order parameters which has a unique values inside the phase and smoothly transitions across the phase interfaces. Since, capillarity is incorporated in the free energy functional through the gradient of the phase-field order parameter, the dynamics of the interface is reproduced in simulations. One can visualize the formation, merging or disappearance of interfaces by taking the relevant physics and mechanisms into consideration.

Phase-field model was first developed by Fix [26] and Langer [27] in 1980s for the study of first-order phase transitions. Ever since, it has gained popularity in the materials science community and has been widely used in various areas like solidification, fracture mechanics and phase transformations. Eguchi et al. studied the kinetics of ordering with phase separation [28] while Collins and Levine used the Cahn-Hilliard equations to develop a diffuse interface model [29]. Caginalp and Fife studied the effect of anisotropy, surface tension, curvature and dynamics of an interface using the phase-field method [30, 31].

In the last couple of years, many industries started using multi-component alloys. To meet this necessity for understanding the morphological and the topological changes in multi-component alloys, Nestler et al. developed a multi-component multiphase-field model to simulate phase transitions and grain coarsening [32]. Choudhury and Nestler introduced the grand potential formulation of the Nestler's multicomponent mutliphase-field model which decoupled the bulk and interface energy contributions and thereby, enabled the large-scale microstructure simulations of phase

transformations in multi-component multiphase alloys [33].

In order to overcome the challenges of experimental approach, the following computational study leverages a phase-field model to understand the behavior of preexisting voids in a monocrystalline copper interconnect. The diffuse interface approach reported in this thesis builds upon the Cahn-Hilliard theory [34, 35] applicable for modeling conserved dynamics of voids which is simulated using the finite difference method and analyzed using numerical post-processing tools.

The main objectives of this study are:

- Devise and validate a phase-field model to study the morphological evolution of voids in metal interconnects.
- Study the effect of electric potential on morphological evolution of void in presence of isotropic atomic mobility.
- Study the effect of electric potential on morphological evolution of void in presence of anisotropic atomic mobility.
- Deduce the effect of surface atomic mobility on the morphological evolution of voids.
- Deduce the role of metal conductivity in modulating the morphological evolution of voids.
- Explore the role of non-uniform electric field on the morphological evolution of voids.

Chapter 2

PHASE-FIELD MODEL

As mentioned above, a diffuse interface model has been used to understand the behavior of circular voids in metal interconnects. The geometry of the system under study is shown in Figure 2.1. The interconnect material and void are distinguished with the help of scaled density ρ which assumes a value of 1 in the metal region and 0 in the void region. The total free energy density of the equation is given by

$$F = \int_V \left[f(\rho) + \kappa_\rho |\nabla \rho|^2 + f_{em} \right] dV \tag{2.1}$$

where $f(\rho)$ represents bulk free energy and the second term is the gradient energy term which ensures a smooth variation in ρ. κ_ρ is the gradient energy coefficient. Bulk free energy can be denoted by

$$f(\rho) = A\rho^2(1-\rho)^2 \tag{2.2}$$

where A is a constant. The electromagnetic force in equation 2.1 can be expressed as

$$f_{em} = eN_A z \rho \phi \tag{2.3}$$

where e is the electronic charge, N_A is Avogadro's number, z is the valence of species undergoing diffusion and ϕ is the electric potential. The temporal evolution of ρ is given by the well-known Cahn-Hilliard equation [34, 35]

$$\partial \rho / \partial t = \nabla \cdot M \nabla \mu \tag{2.4}$$

where,

$$\mu = \delta F / \delta \rho \tag{2.5}$$

is the chemical potential.

In order to account for difference in mobility in various regions of the system, mobility function is given by the equation

$$M(\rho) = M_b + 16 M_s \rho^2 (1-\rho)^2 \tag{2.6}$$

where M_b is the bulk mobility and M_s is the mobility at the surface. Since the present work incorporates anisotropic diffusion in metallic crystals, atomic mobility can be expressed as a second-rank tensor such that its magnitude along the x- and the y-axes can be uniquely defined as M_{xx} and M_{yy}, respectively. Therefore, the mobility tensor, M, is given by

$$\begin{bmatrix} M_{xx} & 0 \\ 0 & M_{yy} \end{bmatrix}. \tag{2.7}$$

In order to couple the physics of electric potential with the phase order parameter, a Laplace equation is used

$$\nabla \cdot [\sigma(\rho)\nabla(\phi)] = 0 \tag{2.8}$$

where σ is the electrical conductivity which is dependent on ρ. By applying a linear interpolation between the metal and void region, we obtain

$$\sigma(\rho) = \sigma_{metal}\rho + \sigma_{void}(1-\rho). \tag{2.9}$$

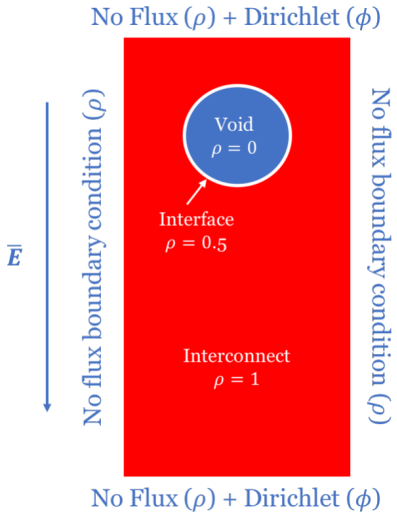

Figure 2.1: A Schematic Diagram Showing the Initial Condition Used for This Study.

All the above equations have been non-dimensionalized by considering the energy scale as $E' = A'$, length scale as $L' = (\kappa'_\rho/A')^{1/2}$ and time scale as $t' = L'^2(\rho'_{metal} - \rho'_{void})^2/M'_b E'$. The ratio of conductivity in metal to the conductivity in void, $\sigma_{metal}/\sigma_{void}$ is denoted by β and the potential difference across the length of interconnect is denoted by ΔV. Unless mentioned otherwise, the electric field in our system is aligned along the y-axis pointing from top to bottom.

To solve the coupled PDEs, an explicit scheme is employed where the spatial and temporal derivatives are discretized using a central difference and the Euler technique, respectively. The Laplace equation is solved iteratively using a successive-over-relaxation (SOR) method. No-flux boundary conditions are applied for q and ρ at the left and right boundaries. Dirichlet boundary conditions are prescribed for/at the top and bottom edges.

Table 2.1 lists down the parameters that we come across in this model and their respective values which have been used in this study.

Parameter	Value
ρ	0 - 1
β	1-10,000
κ_ρ	1
ΔV	2 - 40
M_s	1 - 2
Δt	0.01
Δx	1

Table 2.1: Simulation Parameters Used in This Study.

Chapter 3

MODEL VALIDATION

In order to validate our model, an attempt to reproduce the results of a study conducted by Santoki et al.[24, 36] has been done. In their study, Santoki et al. fixed the values of the co-efficient of surface energy κ_ρ and atomic volume Ω at 1.0, while the ratio of interconnect width to the initial radius of void was fixed at 6.0. Using these parameters, we maintained $\beta = \sigma_{metal}/\sigma_{void}$ at a constant value and varied the potential difference ΔV between 4 and 20 to reproduce their results for isotropic mobility case. For the anisotropic mobility case, we maintained ΔV at a constant value and varied β between 1 and 10,000 as given in their paper. Figures 3.1 and 3.2 show the results that were obtained where the isolines correspond to $\rho = 0.5$.

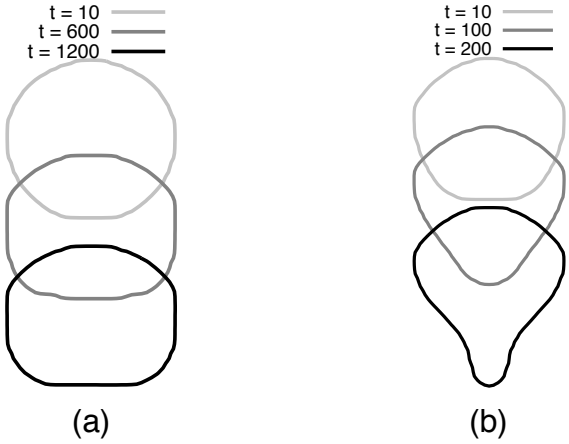

Figure 3.1: Morphological Evolution of a Void Assuming Isotropic Atomic Mobility When Potential Difference, ΔV, is Equal to (a) 4 and (b) 20.

As seen in Figure 3.1, in the case of isotropic mobility of metal atoms, the potential difference, ΔV across the length of the interconnect has a significant effect on the void morphology. At low values of potential difference, there isn't any drastic change in the void morphology. The void slides to the other end, eventually resulting in circuit breakdown. However, when the potential difference across the ends is increased, one can observe that the shape of void changes significantly as the void moves from one end to another.

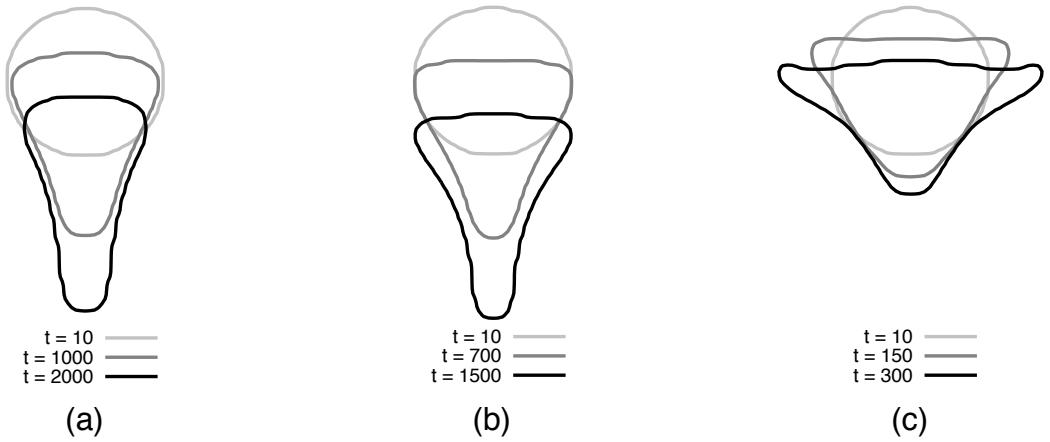

Figure 3.2: Morphological Evolution of a Void Assuming Anisotropic Atomic Mobility When β is Equal to (a) 1, (b) 3 and (c) 10,000.

In the case of anisotropy in the mobility of metal atoms, the value of β plays a very important role. As noted in Figure 3.2, when β value is equal to 1, the void shape changes from a circular one to a long and narrow one. When β is increased to 3, the void becomes broader on the top while it continues to grow and drift towards the other end. When β is increased to 10000, the void becomes wedge-shaped and continues to drift to the other side.

Chapter 4

MORPHOLOGICAL EVOLUTION OF VOID ASSUMING ISOTROPIC ATOMIC MOBILITY

In the following study, we assume the atomic mobility as isotropic to analyze the effects of potential difference, ΔV, surface mobility, M_s, and $\beta = \sigma_{metal}/\sigma_{void}$ on the morphological evolution of the void. Figure 4.1 shows the effect of electric potential on void morphology. As the potential difference across the length of the interconnect is increased, the void develops a protrusion at the bottom as it drifts towards the other end. This protrusion increases in length as time progresses.

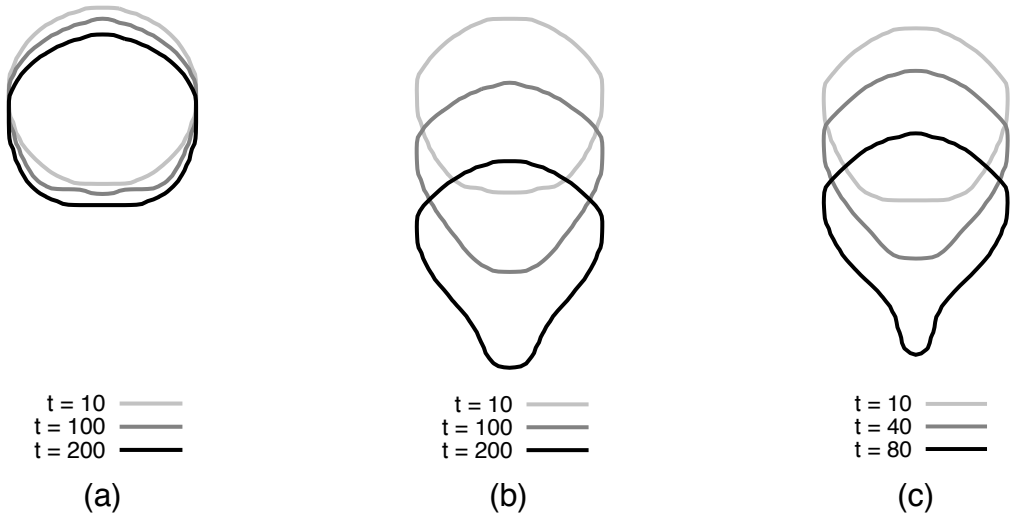

Figure 4.1: Effect of Potential Difference, ΔV, on the Evolution of Void Morphology. Isolines that Are Plotted Correspond to ΔV of (a) 4, (b) 20 and (c) 40.

A larger potential difference implies a stronger electric field. The electrons gain higher momentum and displace metal atoms more easily, increasing the tensile stress at the cathode end. This leads to faster migration of preexisting voids towards the cathode end.

At smaller electric field magnitudes, the displacement of atomic species is faster along the direction of the electric field. This diffusion of atoms causes the void to drift in an opposite direction. However, the capillary force is strong enough to retain the shape of the void to near spherical.

As the electric field becomes stronger, the capillary force is no longer able to

preserve the shape of the void. Atoms along the direction of the applied electric field start diffusing towards the anode more quickly, resulting in a protrusion in void towards the rear end. A change in curvature acts as a driving force for more atoms in that region to diffuse towards the anode, thereby increasing the aspect ratio of the protrusion.

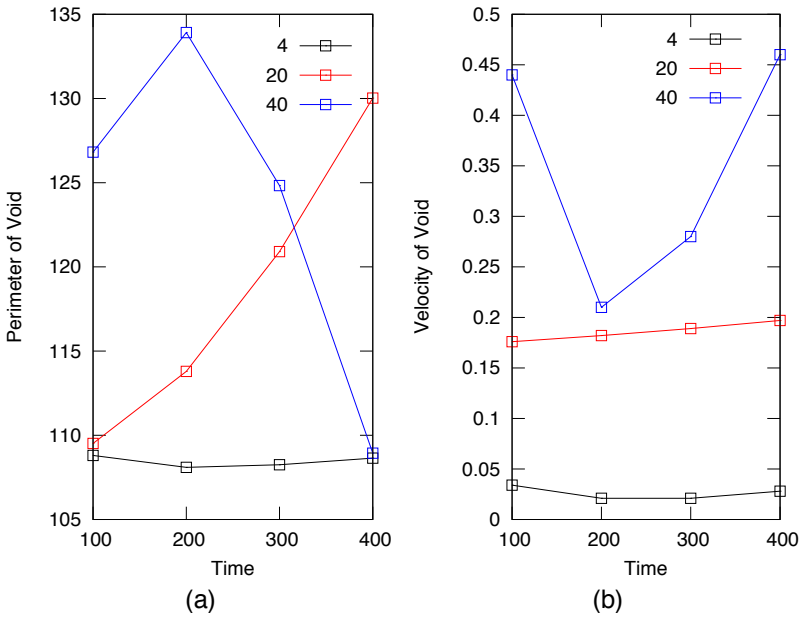

Figure 4.2: Effect of Potential Difference, ΔV, on the Void Kinetics. Plots Showing the Temporal Evolution of Void (a) Perimeter and (b) Velocity for Distinct Values of ΔV.

Figure 4.2 shows void kinetics where perimeter and velocity of the void are plotted with respect to time. As seen in the figure above, the perimeter of the void tends to increase with time. However, when the potential difference is very large, there is a sudden drop in perimeter since a daughter void is formed from the main void. With time, the daughter void pinches off and moves towards the cathode while the parent void starts developing a protrusion again. Since this plot studies the perimeter of the main void alone, there is a decrease in the perimeter.

At smaller values of potential difference, the velocity of void increases slowly with time. However, at a large potential difference, we observe a drop in velocity before it increases again. This might be an effect of counter-acting capillary and electromagnetic forces. Initially, the capillary force predominates the evolution but at a later time, the electromagnetic force establishes complete dominance and the void starts to drift quickly.

As seen in Figure 4.3, as surface mobility is increased, the void drifts faster towards the other end with significant shape change in shape at the rear end. The larger the surface mobility, the larger is the void aspect ratio.

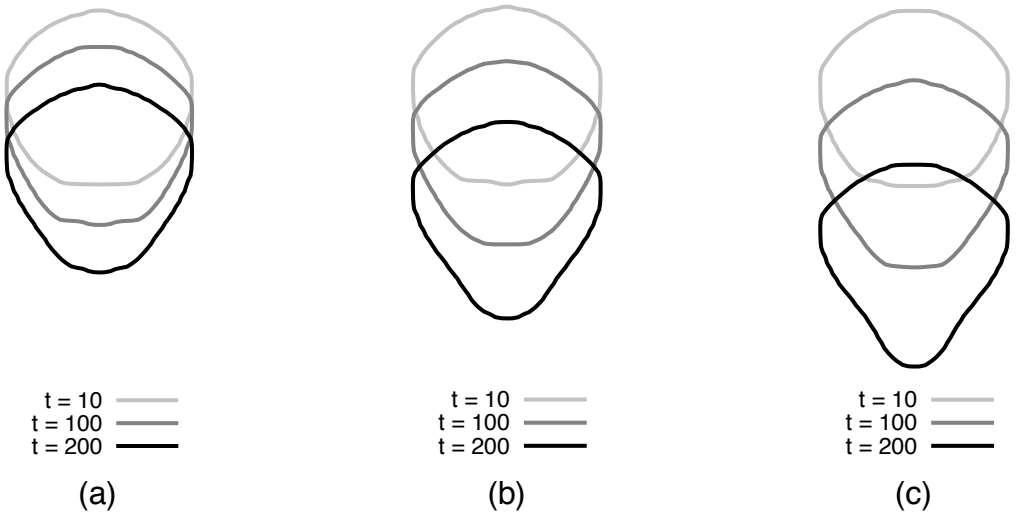

Figure 4.3: Effect of Surface Mobility on Void Kinetics. For the Plotted Isolines Shown above, Surface Mobility, M_s, Equals (a) 1, (b) 1.5 and (c) 2.

Figure 4.4 shows the void kinetics when surface mobility is doubled. For any given value of surface mobility, the aspect ratio of void protrusion, the perimeter of void and the velocity of void increase with time. The velocity of void fluctuates initially due to capillary force trying to reduce the void curvature and surface mobility increasing the protrusion length. However, protrusion length of the void ultimately reaches a stage where it is no longer possible for the capillary force to reduce the curvature,

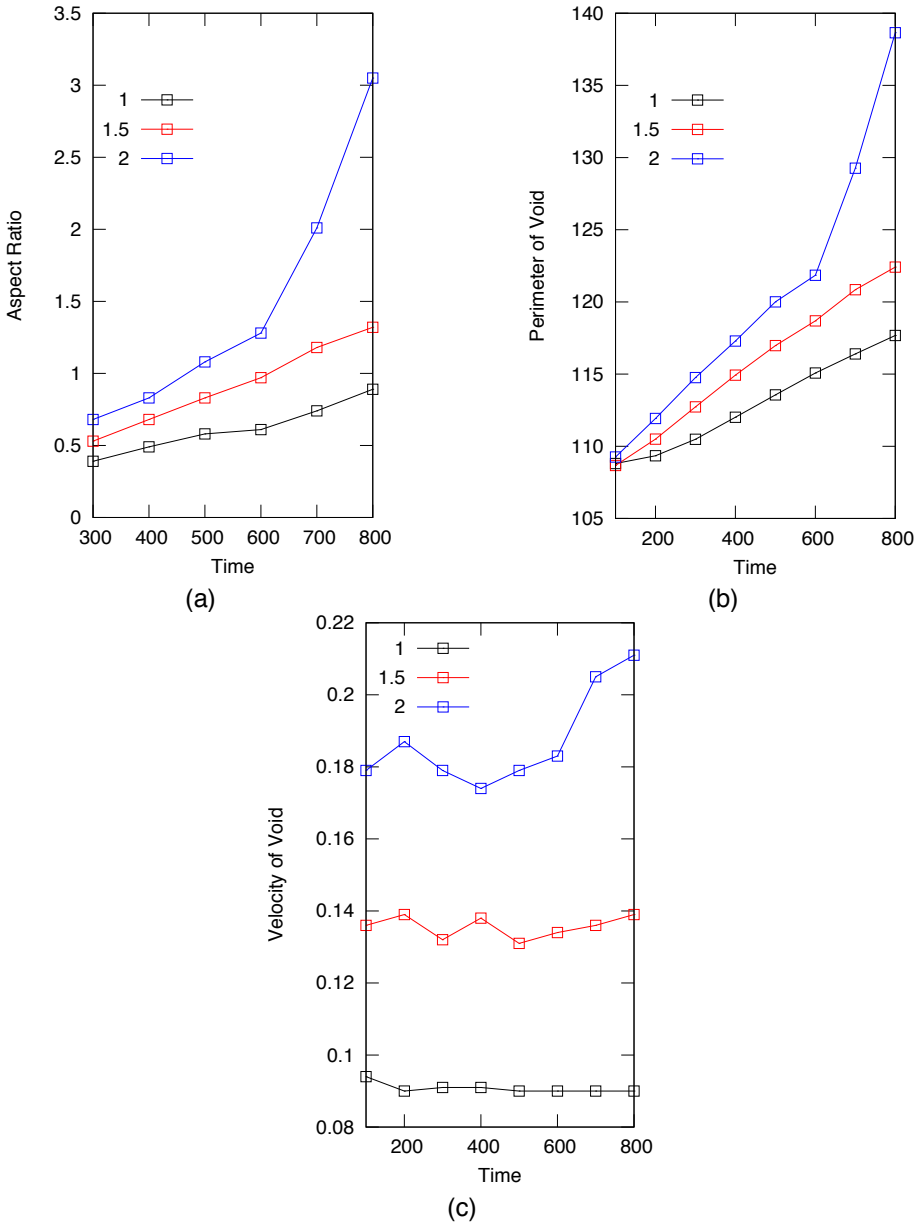

Figure 4.4: Analyzing the Influence of Surface Mobility, M_s, on Void Growth Kinetics. Plots Show Temporal Evolution of Void (a) Aspect Ratio, (b) Perimeter and (c) Velocity for Distinct Values of M_s.

ultimately resulting in an increase in void velocity.

An increase in surface mobility causes the void to drift more quickly. This is due to the fact that a larger surface mobility allows the atoms to diffuse more quickly along

the surface. Similar to the effects seen upon varying electric potential magnitudes earlier, surface mobility also causes the curvature to change at the base and triggers faster diffusion of atomic species along the surface, resulting in a larger aspect ratio of the protrusion. Hence, larger values of surface mobility result in larger void aspect ratios.

Figure 4.5 depicts the effect of β on the temporal evolution of void while Figure 4.6 characterizes void kinetics when β is varied in the range of 10 and 1000.

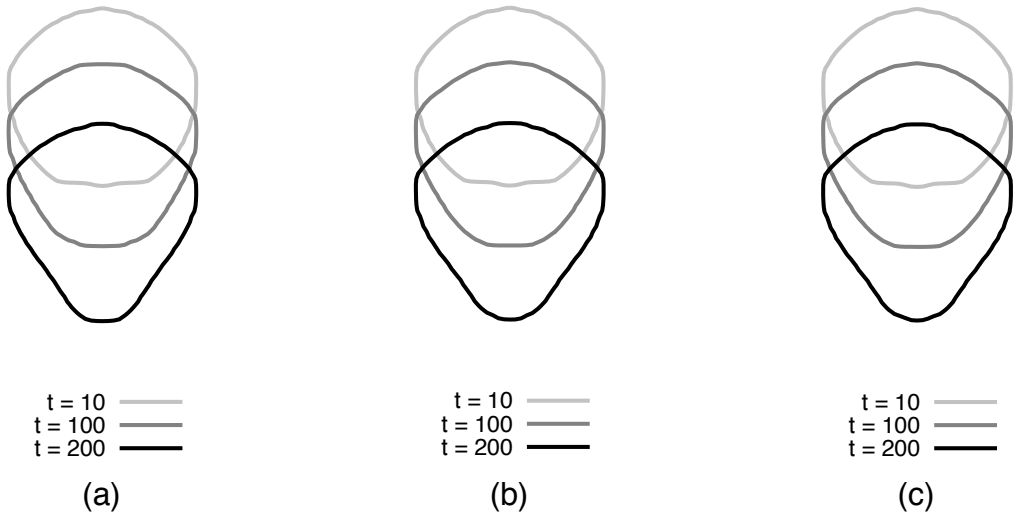

Figure 4.5: Temporal Evolution of Void Morphology When β is Equal to (a) 10, (b) 100 and (c) 1000.

As seen in the Figure 4.5, any significant changes in void morphologies is not observed during the initial timesteps when β is increased from 10 to 1000. For any given value of β, the void starts to increase in size slowly and the protrusion grows with time. At larger timesteps as seen in Figure 4.6 (a), void aspect ratio is found to increase more steeply for smaller value of β. Similar to the previous studies, the velocity of the void fluctuates initially before increasing with time in all the cases.Therefore, increasing β results in significant variation in the late stage evolution characteristics of the void which is in contrast to our observation of early stages.

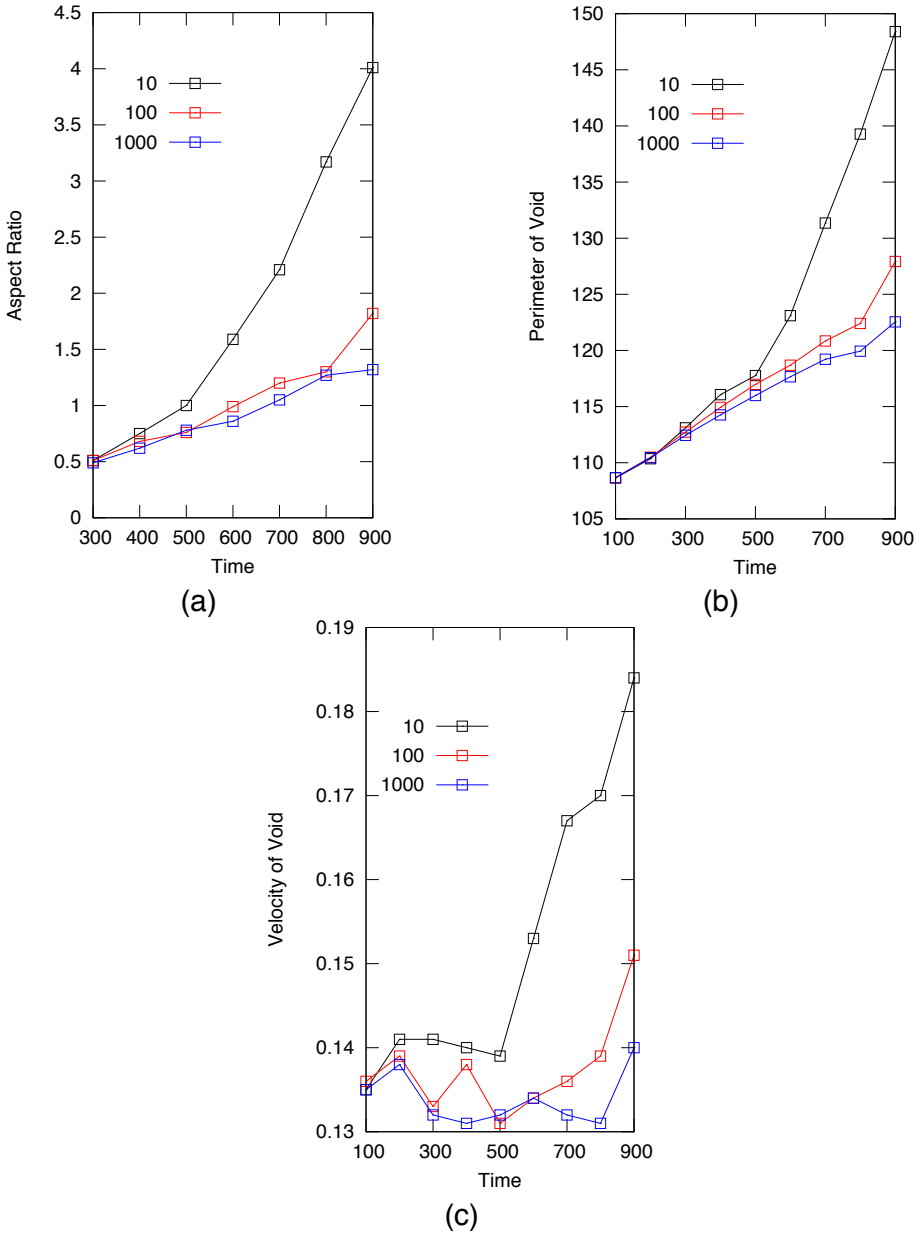

Figure 4.6: Analyzing the Influence of β on Void Kinetics. Plots Showing Temporal Evolution of the Void (a) Aspect Ratio, (b) Perimeter and (c) Velocity for Distinct Values of β Ranging Between 10 and 1000.

Chapter 5

EFFECT OF ANISOTROPIC ATOMIC MOBILITY ON THE MORPHOLOGICAL EVOLUTION OF VOID

In this chapter, we consider the influence of anisotropic atomic mobility in the metallic interconnect. For a detailed understanding, the influence of potential difference ΔV, surface mobility M_s and $\beta = \sigma_{metal}/\sigma_{void}$ have been systematically investigated. For the system under study, mobility is assumed to be greater in the x direction as per the definition in equation 2.7. Figure 5.1 shows the effect of potential difference on void morphology while Figure 5.2 characterizes void evolution kinetics when the potential difference is increased from 2 to 20.

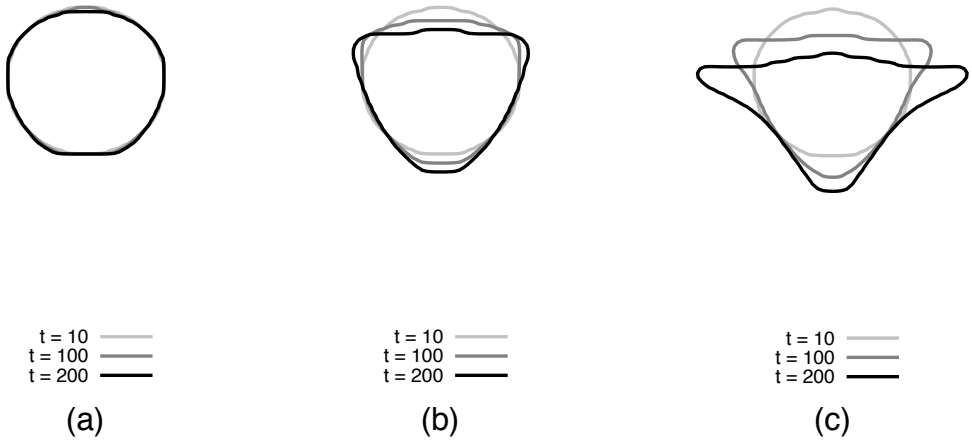

Figure 5.1: Influence of Potential Difference Magnitudes on the Morphological Evolution of Void. The Isolines Correspond to the Temporal Evolution of Void Morphologies Simulated When ΔV Equals (a) 2, (b) 10 and (c) 20.

An increase in potential difference causes the void to broaden at the top while the protrusion becomes long and narrow. Since the mobility of metal atoms is greater in the x direction, this broadening of the void is expected to occur. Similar to the cases when atomic mobility is isotropic, as the potential difference is increased, electromagnetic force becomes stronger than the capillary force and forces atoms to diffuse along the direction of the applied electric field. This results in a protrusion at the rear end which amplifies with time.

At a small value of potential difference, the perimeter of the void increases with

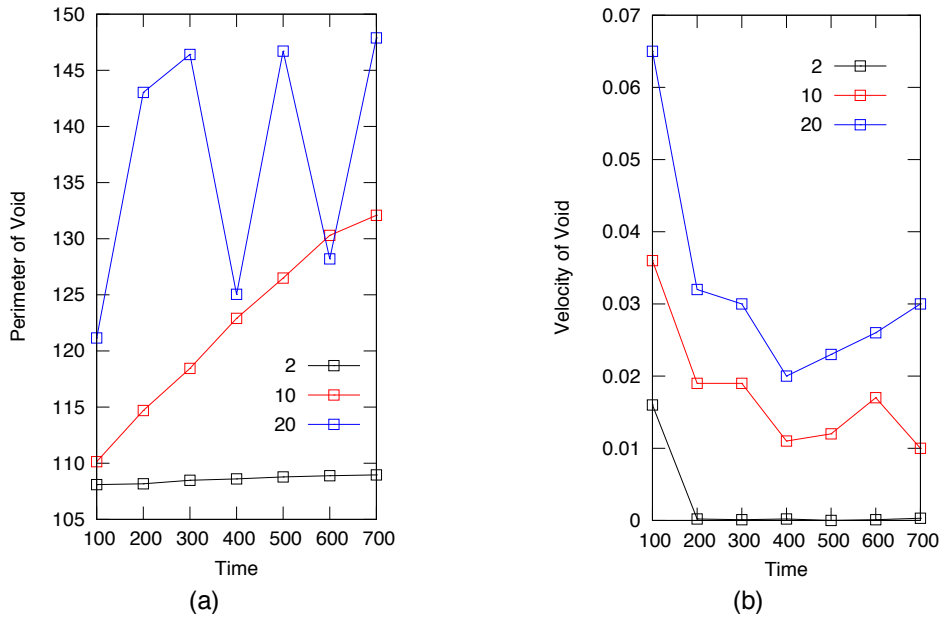

Figure 5.2: Analyzing the Influence of Potential Difference, ΔV, on the Simulated Void Kinetics. Plots Show the Temporal Evolution of Void (a) Perimeter and (b) Velocity for Distinct Values of ΔV Ranging Between 2 and 20.

time. However, when the potential difference is very large, the perimeter of the void fluctuates temporally. We refer to this behavior, as observed in Figure 5.8, as the novel *swimming* void morphology. Here the void morphology fluctuates at a nearly constant frequency as it swims along the length of the interconnect. This is primarily a result of counter-acting (i) capillary force which tries to reduce the curvature of the void, and (ii) anisotropy in atomic mobility along x-axis which is causing the void to broaden. As a result, the perimeter keeps fluctuating while the morphology becomes repetitive. The void velocity, in synergy with its morphology and perimeter, is also found to fluctuate in all the cases.

Figure 5.3 shows the effect of surface mobility on void morphology. As surface mobility is increased, the aspect ratio of protrusion at the rear end of void increases, which is similar to the isotropic case. However, a concomitant broadening of the void

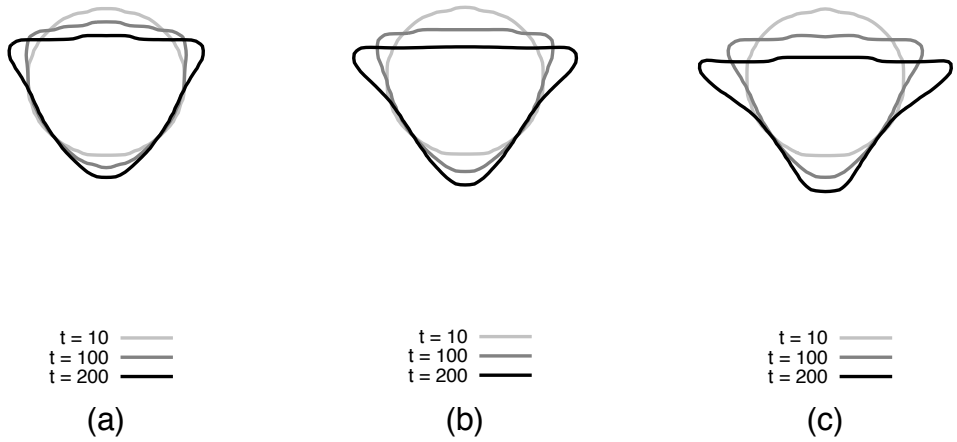

Figure 5.3: Void Morphologies Simulated When Surface Mobility, M_s, is Equal to (a) 1, (b) 1.5 and (c) 2.

along the top surface is also observed due to the larger mobility of atoms in the x direction.

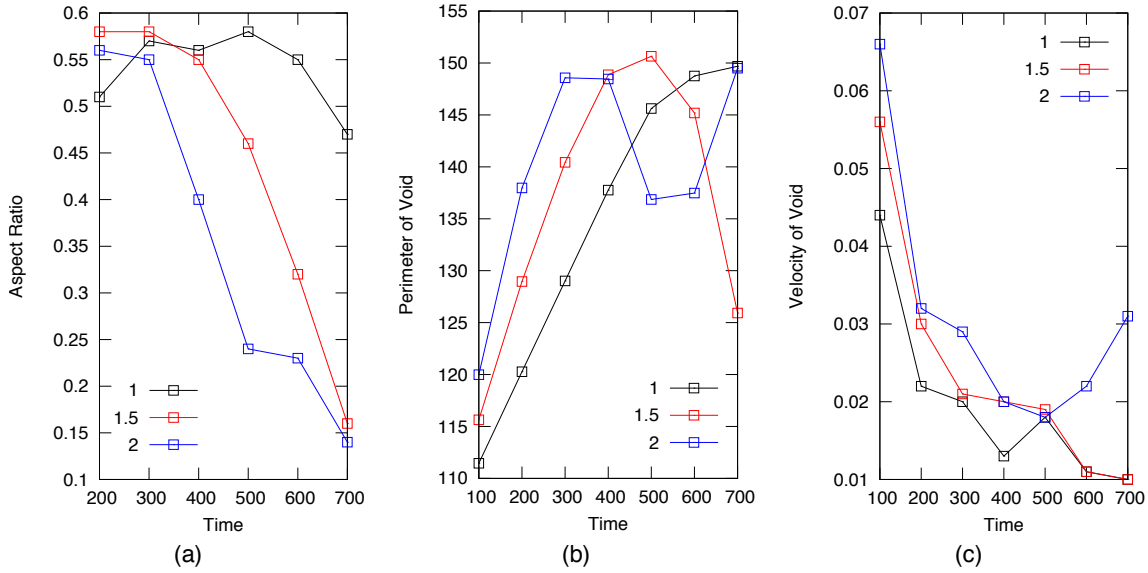

Figure 5.4: Analyzing the Influence of Surface Mobility, M_s, on the Simulated Void Kinetics. Plots Showing the Temporal Evolution of Void (a) Aspect Ratio (b) Perimeter and (c) Velocity at Distinct Values of $M_s = 1, 1.5$ and 2.

Figure 5.4 shows the influence of doubling the magnitude of surface mobility on

the void evolution kinetics. The void kinetics, simulated with anisotropic mobilities, are found to differ with respect to the isotropic cases due to an advent of *swimming* void morphology.

Figure 5.5 shows the effect of β on the void morphologies when mobility is assumed to be anisotropic while the characteristics of void evolution kinetics are plotted in Figure 5.6 . Due to an anisotropic atomic mobility, the atoms diffuse more quickly along the x axis causing the void to broaden in that direction.

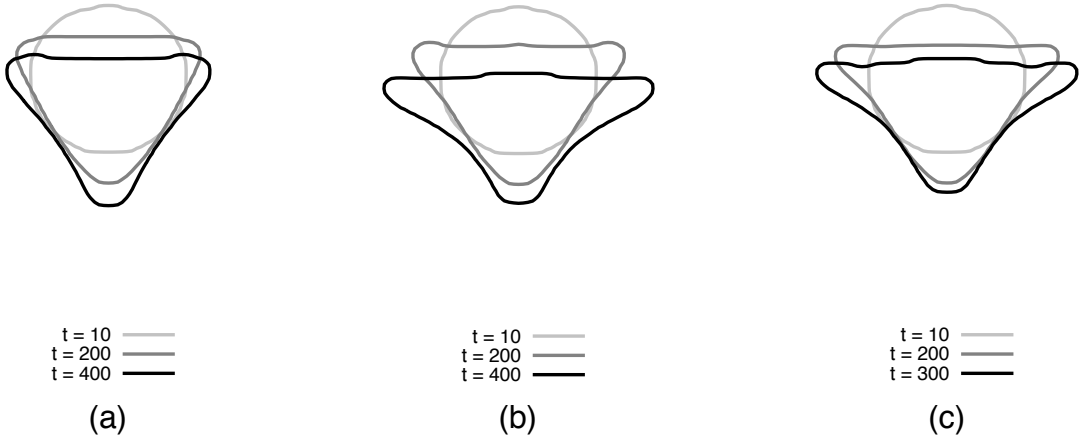

Figure 5.5: Evolution of Void Morphology When β Equals (a) 10, (b) 100 and (c) 1000.

Figure 5.6 clearly show that the void evolution kinetics varies when β is increased from 10 to 1000. Since the swimming void morphology is observed in all the studies with anisotropic mobility, the morphological changes observed in one of the cases is shown in Figure 5.8 (a), where the void morphology is found to be repetitive as it swims along the length of interconnect towards the cathode end. One can argue that the observed *swimming* void morphology is an artifact of the chosen interconnect width which is narrow. Therefore, to verify our novel finding, we simulate the void evolution at larger interconnect widths of 100 Δx to 300 Δx, as shown in Figure 5.7, without altering its length.

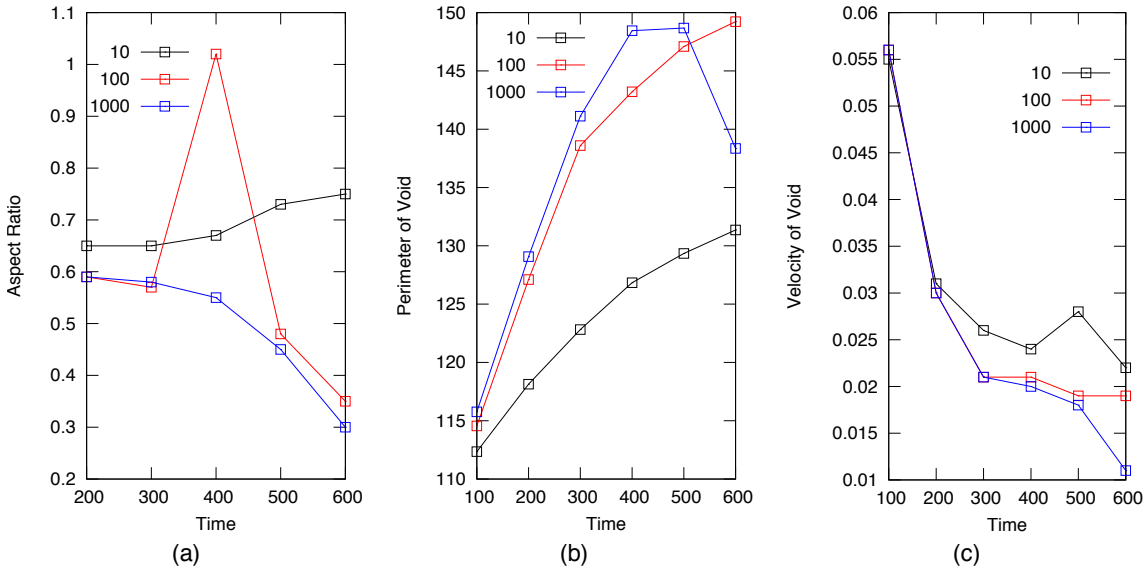

Figure 5.6: Analyzing the Influence of β on the Void Evolution Kinetics. Plots Show Temporal Evolution of Void (a) Aspect Ratio, (b) Perimeter and (c) Velocity for Distinct Values of β that Equal 10, 100 and 1000.

As seen in Figure 5.8, one can observe a swimming void morphology irrespective of the interconnect width. Although the interconnect width does not have any effect on the void morphology, it is important to note that the void drifts (or swims) more quickly when the interconnect width is smaller. This can have serious implications in the semiconductor industry where constant efforts are being made to down-size interconnects in ICs.

In order to understand the void kinetics when interconnect width is increased, the temporal void aspect ratio , perimeter, and velocity are plotted in Figure 5.9. It is evident that at a narrow interconnect width (at $100\Delta x$) significantly influences the void evolution kinetics. However, when the width is increased past 200 Δx to 300 Δx, any significant deviations in void kinetics is not observed. Hence, we can conclude that increasing the interconnect width beyond a certain value will not have any effect on the morphological evolution of the voids.

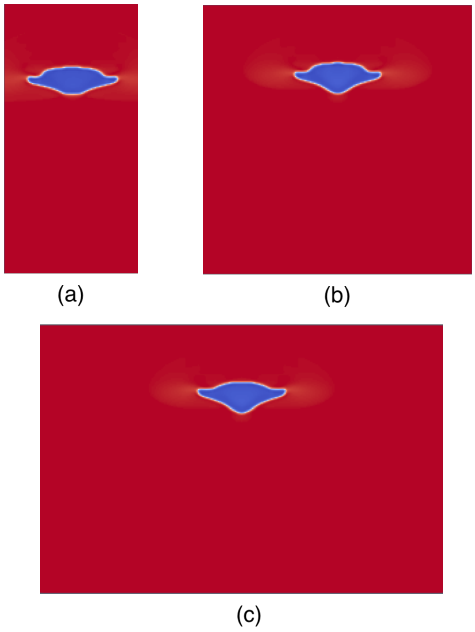

Figure 5.7: Swimming Void Morphologies Simulated at Interconnect Widths of (a) 100 Δx , (b) 200 Δx and (c) 300 Δx.

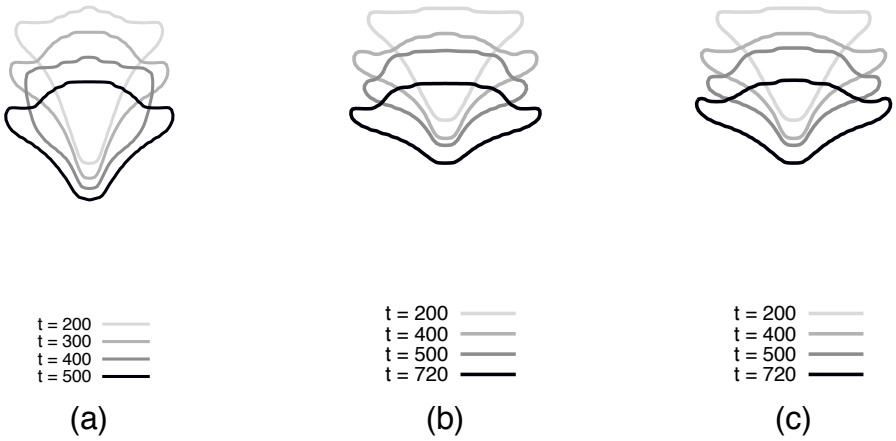

Figure 5.8: Void Morphologies Simulated for Interconnect Widths of (a) 100 Δx , (b) 200 Δx and (c) 300 Δx.

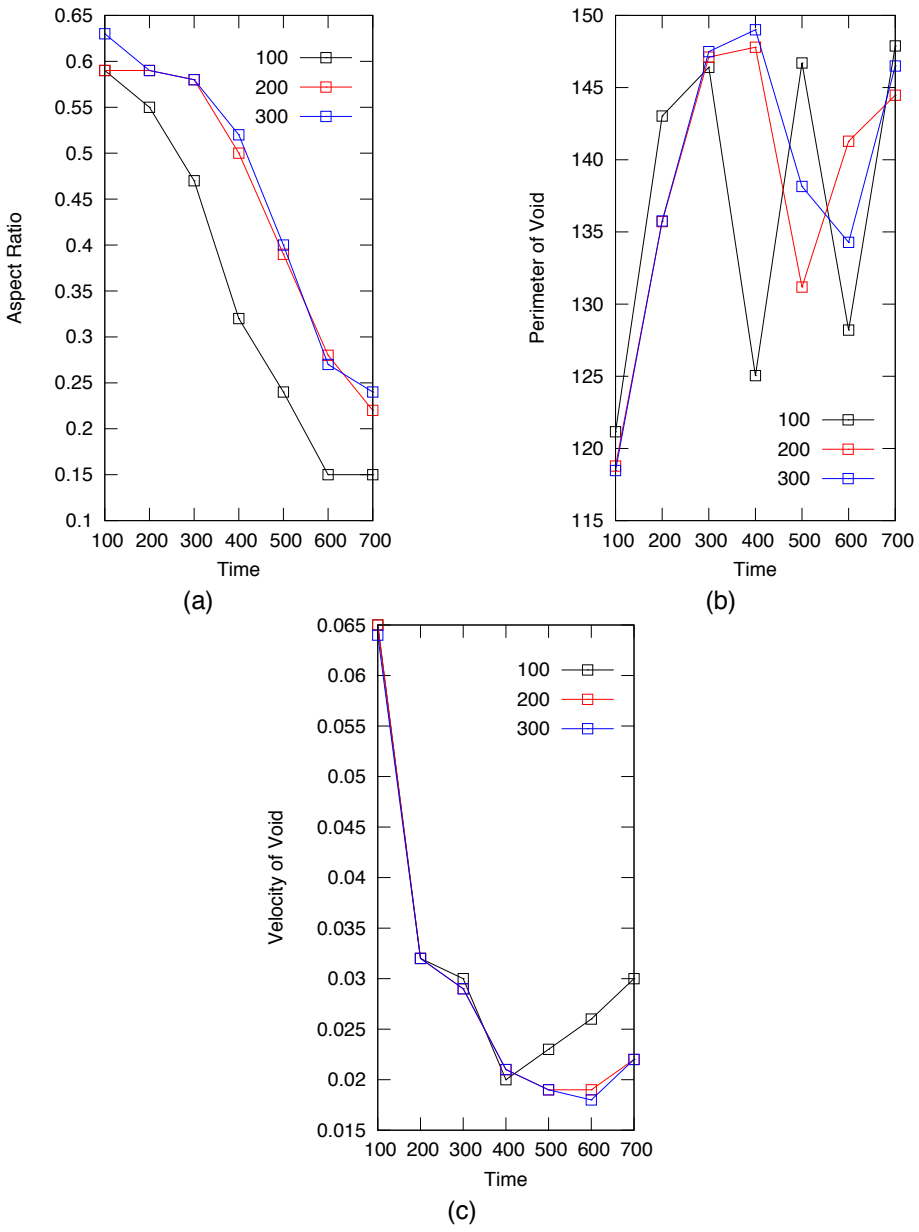

Figure 5.9: Analyzing the Influence of Interconnect Width on the Void Evolution Kinetics. Plots Show the Temporal Evolution of Void (a) Aspect Ratio, (b) Perimeter and (c) Velocity for Distinct Values of Interconnect Widths Corresponding to 100 Δx, 200 Δx and 300 Δx.

Chapter 6

EFFECT OF NON-UNIFORM ELECTRIC FIELD ON THE MORPHOLOGICAL EVOLUTION OF VOID

In this section, we explore the role of a non-uniform electric field on the morphological evolution of voids. The component of the electric field along x-axis (from left to right) is denoted by E_x while along y-axis (from top to bottom), by E_y. For a detailed understanding, we consider the cases pertaining to assumption of isotropic as well as anisotropic atomic mobilities.

Figure 6.1 shows the effect of electric field non-uniformity when the atomic mobility is assumed to be isotropic. When $E_x > E_y$, the void is pushed significantly towards the right-hand side. When the electric field is stronger along the y-axis, the void drifts downwards. When the electric field is equal in magnitude along both the axes, the void moves along 45° with respect to the y-axis.

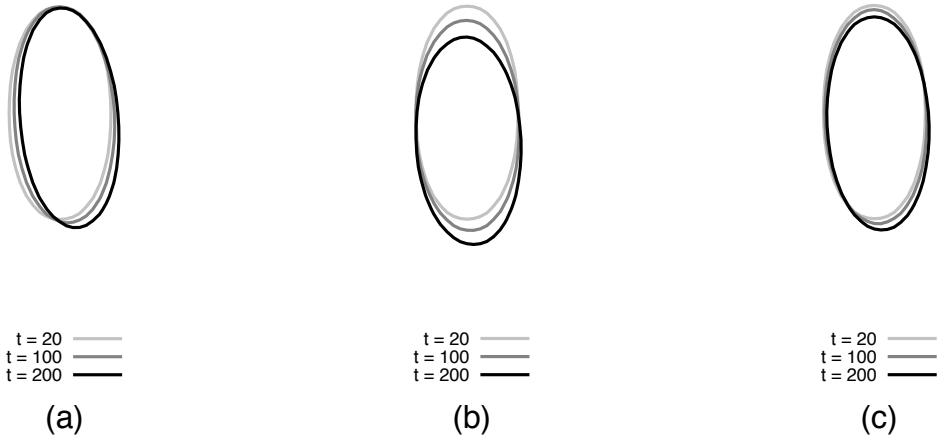

Figure 6.1: Evolution of Void Morphology When (a) $E_x > E_y$, (b) $E_x < E_y$ and (c) $E_x = E_y$. Atomic Mobility is Assumed to be Isotropic.

For the case pertaining to anisotropic mobility, a similar void behavior is observed as shown in Figure 6.2, . However, since the anisotropy is larger along the x direction, the displacement of the void is slightly larger towards the right.

Figure 6.3 confirms the observations stated above by plotting the position of the void center at various time steps. Tables 6.1 and 6.2 show the deviation of void center at a given timestep where $tan\theta$ is a measure of the deviation.

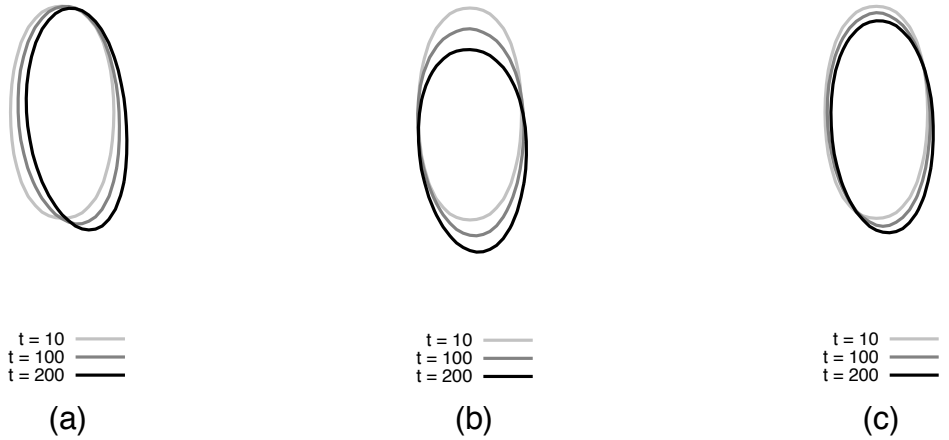

Figure 6.2: Combined Influence of Electric Field Non-Uniformity and Anisotropic Mobility on the Evolution of Void Morphology When (a) $E_x > E_y$, (b) $E_x < E_y$ and (c) $E_x = E_y$.

It is imperative to note that when atomic mobility is assumed to be anisotropic, atoms have a larger mobility along the x-axis as opposed to the y-axis. However, the net displacement of voids is still downwards when $E_x < E_y$, to the right when $E_x > E_y$ and in a diagonal direction when $E_x = E_y$.

As expected, this temporal deviation increases when $E_x > E_y$ for the cases pertaining to isotropic and anisotropic mobilities alike. When $E_x < E_y$, the void drifts at an almost constant rate along a straight line for the case pertaining to isotropic mobility. However, if mobility is assumed to be anisotropic, the deviation fluctuates due to a larger mobility along the x-axis. When $E_x = E_y$, the deviation of void for the case of isotropic mobility is nearly constant along a straight line. However, this deviation temporally in the case of anisotropic atomic mobility.

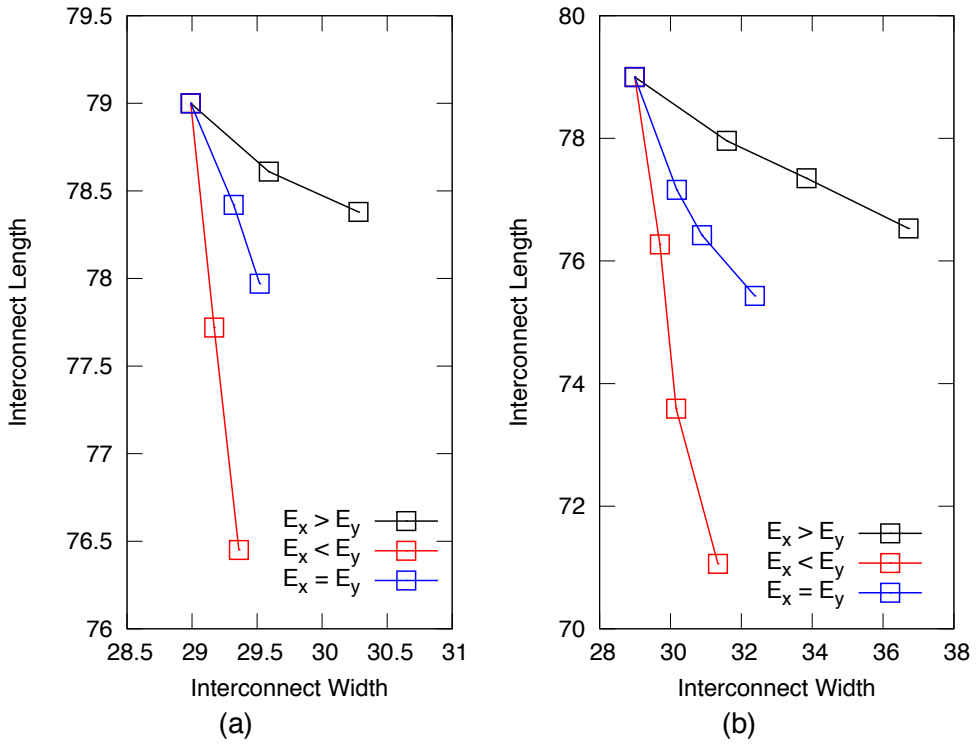

Figure 6.3: Position of Void Center at Intermittent Timesteps Assuming (a) Isotropic and (b) Anisotropic Mobility for Cases Pertaining to $E_x > E_y$, $E_x < E_y$ and $E_x = E_y$.

	Timestep	$tan\theta$
$E_x > E_y$	0	0
	100	1.54
	200	2.08
$E_x < E_y$	0	0
	100	0.12
	200	0.13
$E_x = E_y$	0	0
	100	1.04
	200	1.02

Table 6.1: Deviation of Void Center Assuming Isotropic Mobility When $E_x > E_y$, $E_x < E_y$ and $E_x = E_y$

	Timestep	$tan\theta$
$E_x > E_y$	0	0
	200	2.5
	400	2.94
	600	3.35
$E_x < E_y$	0	0
	200	0.26
	400	0.22
	600	0.29
$E_x = E_y$	0	0
	200	0.65
	400	0.74
	600	0.95

Table 6.2: Deviation of Void Center Assuming Anisotropic Mobility When $E_x > E_y$, $E_x < E_y$ and $E_x = E_y$

Chapter 7

CONCLUSIONS

In this study, a phase-field model has successfully been formulated to analyze the morphological evolution of voids in metal interconnects under electromigration. The effect of isotropic mobility and anisotropic mobility on void behavior have been deduced through an in-depth parametric study.

1. Effect of electric potential on the morphological evolution of void when the atomic mobility is assumed to be isotropic:

• Increase in potential difference across the length of interconnect leads to the formation of a protrusion at the rear end of void which continues to grow in length.

• Rate at which void starts drifting is much larger when the potential difference is increased.

• When the potential difference is very large, a daughter void pinches-out from the parent void, as both continue to drift towards the cathode end.

2. Effect of electric potential on the morphological evolution when the atomic mobility is assumed to be anisotropic:

• Void perimeter and velocity increase when the potential difference across the ends of interconnect is increased.

• Anisotropy in mobility causes the void to broaden on the front end.

• A novel 'swimming void morphology' is observed with a characteristic oscillatory evolution kinetics.

3. Effect of surface mobility on the morphological evolution of void when the atomic mobility is assumed to be isotropic:

• Aspect ratio of void increases with time.

• Void perimeter and velocity increase with time.

• Larger surface mobility causes the void to drift more quickly towards the cathode.

4. Effect of surface mobility on the morphological evolution of void when the atomic mobility is assumed to be anisotropic:

• Aspect ratio of void, void perimeter and velocity increase with time.

• Void drifts more quickly towards the cathode when surface mobility of atoms is increased.

• Anisotropy in mobility results in surface broadening at the front.

• Swimming void morphology is observed in the presence of anisotropic mobility.

5. Effect of $\beta = \sigma_{metal}/\sigma_{void}$ on the morphological evolution when the atomic mobility is assumed to be isotropic:

• There is a notable change in morphological evolution of void when β is increased from 10 to 1000.

• For a particular value of β, aspect ratio of protrusion, void perimeter and void velocity increase with time.

6. Effect of $\beta = \sigma_{metal}/\sigma_{void}$ on the morphological evolution of void when the atomic mobility is assumed to be anisotropic:

• For a given value of β, the aspect ratio of the void, void perimeter and increase with time.

• The void becomes broader at the front face due to anisotropy in the mobility of metal atoms.

• There is a significant change in the void migration kinetics when β in increased from 10 to 1000.

7. Effect of interconnect width on the morphological evolution of void when the atomic mobility is assumed to be anisotropic:

• Interconnect width does not have any effect on the morphology of the evolving void

• At small values of interconnect width, the void drifts more quickly which can have serious implications in the semiconductor industry.

8. Effect of a non-uniform electric field on the void morphology:

• When the atomic mobility is assumed to be isotropic, the net displacement of the void is in the direction of the net electric field.

• When the atomic mobility is assumed to be anisotropic, similar effects are observed in addition to a slightly larger drift along the direction of enhanced mobility.

In the future, we plan on conducting the following studies:

• Understand the reason behind void behavior when β in increased from 10 to 1000.

• Systematically analyze the influence of non-uniform electric field applied at various angles with respect to the x- and the y-axes.

• Increase the number of preexisting voids in the interconnect and study their morphological evolution.

• Incorporate the physics of grain boundaries and extend the model to 3D.

REFERENCES

[1] S. Talukder, P. Kumar, and R. Pratap. Controlled material transport and multidimensional patterning at small length scales using electromigration. *Current Science*, 108:2167–2172, 06 2015.

[2] K.-N. Tu, J.-o. Suh, A. Tzu, C. Wu, N. Tamura, and C.-H. Tung. Mechanism and prevention of spontaneous tin whisker growth. *Materials Transactions*, 46, 11 2005.

[3] A. Mukherjee, K. Ankit, M. Selzer, and B. Nestler. Electromigration-induced surface drift and slit propagation in polycrystalline interconnects: insights from phase-field simulations. *Physical Review Applied*, 9(4):044004, 2018.

[4] S.-k. Lin, Y.-c. Liu, S.-J. Chiu, Y.-T. Liu, and H.-Y. Lee. The electromigration effect revisited: non-uniform local tensile stress-driven diffusion. *Scientific Reports*, 7(1):1–10, 2017.

[5] L. M. Klinger, E. E. Glickman, V. E. Fradkov, W. W. Mullins, and C. L. Bauer. Effect of surface and grain-boundary diffusion on interconnect reliability. *MRS Online Proceedings Library Archive*, 391, 1995.

[6] S. Chakraborty, P. Kumar, and A. Choudhury. Phase-field modeling of grain-boundary grooving and migration under electric current and thermal gradient. *Acta Materialia*, 153:377–390, 2018.

[7] A. E. B. Presland, G. L. Price, and D. L. Trimm. Hillock formation by surface diffusion on thin silver films. *Surface Science*, 29(2):424–434, 1972.

[8] S. K. Sharma and J. Spitz. Hillock formation, hole growth and agglomeration in thin silver films. *Thin Solid Films*, 65(3):339–350, 1980.

[9] Y.-W. Chang, Y. Cheng, L. Helfen, F. Xu, T. Tian, M. Scheel, M. Di Michiel, C. Chen, K.-N. Tu, and T. Baumbach. Electromigration mechanism of failure in flip-chip solder joints based on discrete void formation. *Scientific Reports*, 7(1):1–16, 2017.

[10] H. Mario, M. K. Lim, and C. L. Gan. Impact of pre-existing voids on electromigration in copper interconnects. In *2012 19th IEEE International Symposium on the Physical and Failure Analysis of Integrated Circuits*, pages 1–5. IEEE, 2012.

[11] Z. Tang and F. G. Shi. Effects of preexisting voids on electromigration failure of flip chip solder bumps. *Microelectronics Journal*, 32(7):605–613, 2001.

[12] S. B. Liang, C. B. Ke, W. J. Ma, M. B. Zhou, and X. P. Zhang. Numerical simulations of migration and coalescence behavior of microvoids driven by diffusion and electric field in solder interconnects. *Microelectronics Reliability*, 71:71–81, 2017.

[13] T.-Y. Hsu, J.-Y. Chang, H.-M. Chang, and F.-Y. Ouyang. Electromigration induced spontaneous Ag whisker growth in fine Ag-alloy bonding interconnects: Novel polarity effect. *Materials Letters*, 182, 06 2016.

[14] C. L. Gan and M. K. Lim. 5 - voiding in copper interconnects during electromigration. In Choong-Un Kim, editor, *Electromigration in Thin Films and Electronic Devices*, Woodhead Publishing Series in Electronic and Optical Materials, pages 113 – 134. Woodhead Publishing, 2011.

[15] R. L. [de Orio], H. Ceric, and S. Selberherr. A compact model for early electromigration failures of copper dual-damascene interconnects. *Microelectronics Reliability*, 51(9):1573 – 1577, 2011. Proceedings of the 22th European Symposium on the Reliability of electron devices, failure physics and analysis.

[16] A. Adhikari and A. Roy. Experimenting and modeling of catastrophic failure in electromigration-induced resistance degradation for deep submicron dual-damascene copper interconnects. *Solid-State Electronics*, 148:7–15, 2018.

[17] Z. Sun, E. Demircan, M. D. Shroff, C. Cook, and S. X-D Tan. Fast electromigration immortality analysis for multisegment copper interconnect wires. *IEEE Transactions on Computer-Aided Design of Integrated Circuits and Systems*, 37(12):3137–3150, 2018.

[18] A. A. Khomich, A. P. Bolshakov, E. E. Ashkinazi, A. V. Khomich, R. A. Khmelnitsky, V. G. Ralchenko, and V. I. Konov. Optical spectroscopy characterization of growth hillocks on the surface of homoepitaxial CVD diamond films. *Journal of Physics: Conference Series*, 1199:012006, mar 2019.

[19] S. Liu, C. Chen, P. Liu, and T. Chou. Tin whisker growth driven by electrical currents. *Journal of Applied Physics*, 95:7742–7747, 06 2004.

[20] Y. Jung and J. Yu. Electromigration induced kirkendall void growth in sn-3.5 ag/cu solder joints. *Journal of Applied Physics*, 115(8):083708, 2014.

[21] C. W. Chang, C. V. Thompson, C. L. Gan, K. L. Pey, W. K. Choi, and Y. K. Lim. Effects of microvoids on the linewidth dependence of electromigration failure of dual-damascene copper interconnects. *Applied Physics Letters*, 90(19):193505, 2007.

[22] T. Frolov, W. J. Boettinger, and Y. Mishin. Atomistic simulation of hillock growth. *Acta Materialia*, 58(16):5471 – 5480, 2010.

[23] A. Mukherjee, K. Ankit, R. Mukherjee, and B. Nestler. Phase-field modeling of grain-boundary grooving under electromigration. *Journal of Electronic Materials*, 45(12):6233–6246, 2016.

[24] J. Santoki, A. Mukherjee, D. Schneider, M. Selzer, and B. Nestler. Phase-field study of electromigration-induced shape evolution of a transgranular finger-like slit. *Journal of Electronic Materials*, 48(1):182–193, 2019.

[25] L. Klinger and L. Levin. Interface instability in an electric field. *Journal of Applied Physics*, 78(3):1669–1672, 1995.

[26] G. J. Fix. Phase field methods for free boundary problems. 1982.

[27] J. S. Langer. *Models of pattern formation in first-order phase transitions*, pages 165–186.

[28] T. Eguchi, K. Oki, and S. Matsumura. Kinetics of ordering with phase separation. *MRS Online Proceedings Library Archive*, 21, 1983.

[29] J. B. Collins and H. Levine. Diffuse interface model of diffusion-limited crystal growth. *Physical Review B*, 31:6119–6122, May 1985.

[30] G. Caginalp and P. Fife. Phase-field methods for interfacial boundaries. *Physical Review B*, 33:7792–7794, Jun 1986.

[31] G. Caginalp and P. Fife. Higher-order phase field models and detailed anisotropy. *Physical Review B*, 34:4940–4943, Oct 1986.

[32] B. Nestler, H. Garcke, and B. Stinner. Multicomponent alloy solidification: Phase-field modeling and simulations. *Physical Review E*, 71:041609, Apr 2005.

[33] A. Choudhury and B. Nestler. Grand-potential formulation for multicomponent phase transformations combined with thin-interface asymptotics of the double-obstacle potential. *Physical Review E*, 85:021602, Feb 2012.

[34] J.W. Cahn and J.E. Hilliard. Free energy of a nonuniform system. I. Interfacial free energy. *The Journal of Chemical Physics*, 28(2):258–267, 1958.

[35] J.W. Cahn. On spinodal decomposition. *Acta Metallurgica*, 9(9):795–801, 1961.

[36] J. Santoki, A. Mukherjee, D. Schneider, and B. Nestler. Role of conductivity on the electromigration-induced morphological evolution of inclusions in {110}-oriented single crystal metallic thin films. *Journal of Applied Physics*, 126(16):165305, 2019.